Stability of Dynamically Propagating Cracks in Brittle Materials

by

K. Uenishi

Division of Engineering and Applied Sciences and Department of Earth and Planetary Sciences

Harvard University

Cambridge, Massachusetts, USA

and

H.P. Rossmanith

Institute of Mechanics, Vienna University of Technology

Vienna, Austria

Acta Mechanica, No.156(3-4), pp.179-192, 2002.

Abstract

Dynamic crack propagation and bifurcation phenomena are investigated analytically by utilizing the strain energy density fracture criterion in the framework of catastrophe theory. The effect of biaxial stress, loading imperfections (mixed-mode loading), Poisson's ratio, state of stress as well as crack tip propagation speed on the crack path directional stability is analyzed. Special crack path stability charts for (un)stably propagating cracks are obtained and their connection with the experimentally recorded crack tip stress field is addressed. It is shown that slight change of the normal stress acting parallel to a crack at its tip (crack-parallel stress) may be able to affect the crack surface roughening and/or branching velocity considerably. It is also indicated that under small tensile crack-parallel stress, the crack propagation is stable only when the crack propagation speed is less than about 30% of the relevant shear wave speed. The crack becomes unstable and its surfaces roughen severely at a higher speed, and the crack bifurcates at the highest propagation speed, some 45% of the shear wave speed. It is suggested that superimposing mode-II (shear) loading will enhance the dynamic crack path stability while increasing crack propagation speed will reduce the stability of crack propagation. It is expected that under compressive crack-parallel stress, no crack surface roughening will occur before the crack stably bifurcates.

Keywords: crack branching and bifurcation, dynamic fracture, crack propagation, crack mechanics, energy methods, stability and bifurcation, catastrophe theory, loading imperfection.

1. Introduction

The investigation into the fundamental mechanical behavior of cracks prior and subsequent to a critical point of stability has been of great importance in understanding the rupture mechanism of brittle solids, and therefore it has been the subject of numerous researches (see e.g. [1], [2]). The theoretical analyses of a crack extending on a plane have shown that under typical mode-I and II remote loading conditions the limiting propagation speed of a crack tip c is the Rayleigh wave speed, c_R, of the material. However, laboratory experiments and observations suggest that when a crack extends in brittle materials under suitable stress conditions and its velocity exceeds a certain limit, it oscillates (surface roughening) and subsequently divides into two or more branches. For a mode-I crack in brittle amorphous solids (glass, PMMA), the crack propagation speed c has an upper limit of order 0.5-0.6c_S (0.55-0.65c_R). Here, c_S is the relevant shear wave speed in that solid. The fracture surface is mirror-smooth only for c < 0.27-0.36c_S (0.3-0.4c_R). The crack surface roughens severely at higher speeds and the crack bifurcates at the highest speeds [3]-[6].

The attempts to explain the observed low limiting speeds and the crack surface roughening have started with the work by Yoffe [7]. She solved the elastodynamic equations for a running crack of finite length, showing the dependency of the structure of the near tip singular field on the crack propagation speed, c, and found that, when c > 0.6c_S (0.65c_R), the circumferential normal stress at a fixed small radius $r = r_0$ from the tip (within the singularity-dominated area) reaches a maximum at an angle $\theta \neq 0$ with respect to the current crack growth direction. This result may give a plausible explanation of limiting speeds and macroscopic branching, but does not explain the surface roughening that can occur at much smaller speeds [6]. By assuming sudden change of rupture speed just before and just after bifurcation, Freund [8] showed that the limiting speed for a mode-I crack is $c \approx 0.45c_S$ (0.5c_R). However, even if the

change of speed of a fracture before and after branching is properly incorporated, it seems unlikely that the onset of crack surface roughening at speeds in the range $c \approx 0.27\text{-}0.36c_S$ (0.3-0.4c_R) can be explained by a branching instability at a crack tip [6].

An alternative approach to the crack stability problem may be based on the analysis of crack path directional stability. Close observations into experimentally recorded wave patterns indicate that the characteristics of crack propagation depend essentially on and may be controlled by the loading conditions that are basically influenced by the geometrical configuration of the specimen [1], [9]-[12], and it has been noticed that the normal uniform stress acting parallel to a crack at its tip (crack-parallel stress) considerably affects the path stability of an extending crack. Analytically, using the symmetry condition of vanishing mode-II stress intensity factor $K_{\mathrm{II}} = 0$ for crack growth direction, Melin [13]-[14] considered the directional stability of a static crack subjected to biaxial remote loading $\sigma_x = \sigma_x^{\infty}$ (crack-parallel stress) and $\sigma_y = \sigma_y^{\infty}$ (crack-normal stress), and showed that the directional instability occurs for $\sigma_x^{\infty} / \sigma_y^{\infty} > 1$, but, irrespective of the crack length, the crack edges actually move away from the original crack plane if $\sigma_x^{\infty} / \sigma_y^{\infty} \geq 1 - \pi/4 \approx 0.2146$. Therefore, the question of crack directional stability cannot be answered by considering only a crack edge vicinity, for example by analyzing the effect of an initial disturbance near the edge of a semi-infinite crack, using the stability criterion that the crack edge should move towards the original crack plane like in [15]: the positive T-stress (which for a mode-I crack in a large plate implies that $\sigma_x^{\infty} / \sigma_y^{\infty} > 1$) cannot be a criterion for directional stability [1]. This suggests that cracking is not a purely local phenomenon and a more global criterion should be used. It should also be noted that although the criteria for the direction of crack growth [16]:

$$K_{\mathrm{I}}(\theta) = \textit{maximum} \quad \text{or} \quad K_{\mathrm{II}}(\theta) = 0, \tag{1}$$

especially the second criterion, have been extensively used in numerical schemes, these criteria are equivalent only for a crack propagating under smoothly changing direction. For a stationary crack subjected to mixed mode loading ($K_{II} \neq 0$), the angle that maximizes K_I differs from the one for $K_{II} = 0$. The simple symmetry condition $K_{II} = 0$ is, in general, less reliable when small scale yielding cannot be assumed [1], for instance, around the tips of a dynamically propagating crack where excessively large fracture process zones and resulting crack division may be expected.

Therefore, in this study, the strain energy density fracture criterion, together with the catastrophe theory, will be employed to analyze the dynamic crack path stability and branching under mixed-mode conditions. The reasons for using the strain energy density criterion are: (1) it is simple to be applied; (2) the core region (a certain area around a crack tip where the singular stresses would occur) is excluded, and more globally, the exterior (but very close) field is considered; and (3) the analytical results often match the experimental findings, especially when cracks are under mixed-mode loading. There is a reference radius that deserves a physical interpretation in this criterion. However, such reference radii appear even when we employ the stress intensity factor *K*-based criteria (including the maximum tensile stress or shear stress criterion).

2. The State of Stress around a Crack Tip and the Strain Energy Density

2.1. *Analytical basis*

Consider the arbitrary motion of a crack tip in the ξ,η-plane subjected to a general exterior stress field except that the crack speed is always less than the characteristic Rayleigh wave velocity, c_R. The local Cartesian (x, y) as well as a local polar coordinate system (r, θ) are

attached with the crack tip P(ξ, η) such that the crack velocity vector is parallel to the *x*-direction which also coincides with $\theta = 0$ (see Fig.1).

The plane elastodynamic crack tip stress field for running cracks can be represented in the form [2], [17]-[18]:

$$\sigma_{ij} = \frac{K_{\mathrm{I}}}{\sqrt{2\pi r}} f_{ij}^{I}(c,\theta) + \frac{K_{\mathrm{II}}}{\sqrt{2\pi r}} f_{ij}^{II}(c,\theta) + \sigma_x^{\infty}\delta_{i1}\delta_{1j} + O(1)\ , \tag{2}$$

where c is the crack tip speed, K_{I} and K_{II} denote the mode-I and mode-II dynamic stress intensity factors, and σ_x^{∞} is a uniform normal stress acting parallel to the crack line $\theta = 0$ (crack-parallel stress). The functions $f_{ij}^{I}(c,\theta)$ and $f_{ij}^{II}(c,\theta)$ depend on the crack speed c and the angular coordinate θ:

$$\begin{cases} f_{11}^{I} = B^{I}\left[(1+2\alpha_P^2-\alpha_S^2)\dfrac{\cos(\theta_P/2)}{\sqrt{r_P}} - \dfrac{4\alpha_P\alpha_S}{1+\alpha_S^2}\dfrac{\cos(\theta_S/2)}{\sqrt{r_S}}\right], \\ f_{12}^{I} = 2B^{I}\alpha_P\left[\dfrac{\sin(\theta_P/2)}{\sqrt{r_P}} - \dfrac{\sin(\theta_S/2)}{\sqrt{r_S}}\right], \\ f_{22}^{I} = B^{I}\left[-(1+\alpha_S^2)\dfrac{\cos(\theta_P/2)}{\sqrt{r_P}} + \dfrac{4\alpha_P\alpha_S}{1+\alpha_S^2}\dfrac{\cos(\theta_S/2)}{\sqrt{r_S}}\right], \\ f_{11}^{II} = B^{II}\left[-(1+2\alpha_P^2-\alpha_S^2)\dfrac{\sin(\theta_P/2)}{\sqrt{r_P}} + (1+\alpha_S^2)\dfrac{\sin(\theta_S/2)}{\sqrt{r_S}}\right], \\ f_{12}^{II} = B^{II}\left[2\alpha_P\dfrac{\cos(\theta_P/2)}{\sqrt{r_P}} - \dfrac{(1+\alpha_S^2)^2}{2\alpha_S}\dfrac{\cos(\theta_S/2)}{\sqrt{r_S}}\right], \\ f_{22}^{II} = B^{II}(1+\alpha_S^2)\left[\dfrac{\sin(\theta_P/2)}{\sqrt{r_P}} - \dfrac{\sin(\theta_S/2)}{\sqrt{r_S}}\right], \end{cases} \tag{3}$$

where

$$\begin{cases} B^I = \dfrac{(1+\alpha_S^2)\sqrt{r}}{D},\ B^{II} = \dfrac{2\alpha_S\sqrt{r}}{D},\ D = 4\alpha_P\alpha_S - (1+\alpha_S^2)^2, \\ \alpha_P = \sqrt{1-\dfrac{c^2}{c_P^2}},\ c_P : \text{longitudinal wave speed}, \\ \alpha_S = \sqrt{1-\dfrac{c^2}{c_S^2}},\ c_S : \text{shear wave speed}, \\ r_P e^{i\theta_P} = x + i\alpha_P y,\ r_S e^{i\theta_S} = x + i\alpha_S y. \end{cases} \tag{4}$$

In the following analysis, all regular stress fields [incorporated in $O(1)$] will be neglected.

For the investigation of the multi-parametric problems of crack propagation within the framework of the catastrophe theory, the elastic strain energy density W of the stress field around a crack tip will be employed as a potential function. For plane problems the strain energy density W may be expressed as the sum of an isochromatic and an isopachic contribution:

$$W = \frac{1}{16\mu}[8\tau_m{}^2 + (\kappa-1)I^2], \tag{5}$$

where μ is shear modulus, τ_m is maximum shear stress, $I = \sigma_x + \sigma_y$ (sum of normal stresses), $\kappa=3-4\nu$ for plane strain and $\kappa=(3-\nu)/(1+\nu)$ for plane stress, and ν is Poisson's ratio. The form of equ.(5) implies a strong correlation between the shapes of equi-strain-energy-density lines and isochromatics and isopachics observed in laboratory experiments.

With the abbreviations:

$$\begin{cases} F = f_{22}^I - f_{11}^I + m(f_{22}^{II} - f_{11}^{II}), \\ G = 2(f_{12}^I + m f_{12}^{II}), \\ H = f_{22}^I + f_{11}^I + m(f_{22}^{II} + f_{11}^{II}), \end{cases} \tag{6}$$

where $m = K_{II} / K_I$, the expression for the strain energy density W takes the form

$$W = \frac{K_I^2}{16\pi\mu r}\left[(F-\alpha^*)^2 + G^2 + \frac{\kappa-1}{2}(H+\alpha^*)^2\right]. \tag{7}$$

Here the new variable $\alpha^* = \alpha\sqrt{r/r_0}$ with $\alpha = \sigma_x^\infty\sqrt{2\pi r_0}\,/K_I$ has been introduced. The quantity r_0 represents a reference radius [9].

2.2. *The effect of the crack-parallel stress observed in laboratory experiments*

The effect of the crack-parallel stress on crack path stability can be seen clearly in laboratory experiments using a Double-Cantilever-Beam (DCB) specimen [Fig.2(a)] and a Single-Edge-Notched (SEN) specimen [Fig.2(b)]. It is expected that a DCB specimen will give positive (tensile) crack-parallel stress while an SEN specimen will render negative (compressive) normal stress acting parallel to the crack surface. Dynamic photoelasticity is utilized to experimentally record the isochromatic crack tip fringe patterns (lines of constant maximum shear stress, τ_m).

The photographs in Figs.3 and 4 show the isochromatic fringe patterns associated with a dynamically propagating crack (c/c_S = 0.2) in Homalite 100 subjected to mode-I [(a) in each figure] and mixed-mode [(d) in each figure] loading conditions in a DCB specimen (Fig.3) and in an SEN specimen (Fig.4). Figure 3(a) pertains to the case where the crack, under pure mode-I loading, is subjected to tensile crack-parallel stress, and clearly shows, even under a relatively small crack tip speed c/c_S = 0.2, an unstable crack path behind the tip. However, if a loading imperfection, or mode-II shear loading, is superimposed to the crack, then, as seen in Fig.3(d), the crack propagates stably and smoothly. The photographs in Fig.3 show that adding mode-II loading will enhance the stability of the dynamic crack path. The corresponding isochromatic fringe patterns, generated analytically using the formulae described above, are depicted in Figs.3(b) and (e), and equi-strain-energy-density lines are shown in Figs.3(c) and (f) for the same fracture test specimen, DCB. The local minima and maxima directions related to the maximum shear stress and the strain energy density are indicated by the markers (dots and short lines) in these figures.

Figure 4(a) and (d) show that under compressive crack-parallel stress, the crack can propagate stably, without surface roughening. The corresponding, analytically obtained isochromatic fringe patterns and equi-strain-energy-density lines are indicated also in Fig.4. The

markers (dots and short lines) in these figures show the directions of local minima and maxima. Notice the strong effect of the crack-parallel stress σ_x^{∞} (or α, α^*) onto the tilt angle of isochromatic loops [backward leaning loops for a DCB specimen (Fig.3), forward leaning loops for an SEN specimen (Fig.4)] and also onto the shape of equi-strain-energy-density lines. Comparison of Fig.4(a) with Fig.3(a) suggests that the normal stress acting parallel to a crack at its tip may be able to affect the crack stability: negative (compressive) crack-parallel stress enhances the stability of a dynamically propagating crack while positive (tensile) crack-parallel stress tends to reduce the crack stability and may induce crack surface roughening.

3. Crack Path Directional Stability and Crack Branching

The stability of crack path is discussed analytically in more detail using the strain energy density fracture criterion. This criterion is based on the exploration of the equi-strain-energy-density line pattern around the crack tip. Application of the catastrophe theory [19] in connection with the principle of crack propagation along the minima of the elastic strain energy density allows for the construction of stability charts on the basis of the extreme values of the strain energy density [9]-[11]:

$$\partial W/\partial\theta = 0, \quad \text{for } r = r_n \text{ and } \theta = \theta_n \tag{8}$$

Combination of equ.(7) with the condition (8) renders the governing equation for the general mixed-mode stability chart:

$$\alpha^* = \alpha\sqrt{\frac{r_n}{r_0}} = \frac{\sigma_x^{\infty}\sqrt{2\pi r_n}}{K_{\mathrm{I}}} = \frac{2(F\dot{F}+G\dot{G})+(\kappa-1)H\dot{H}}{2\dot{F}-(\kappa-1)\dot{H}} \ . \tag{9}$$

Here, $(\,)^{\bullet} = \partial(\,)/\partial\theta$. A crack is directionally stable provided that $\partial^2 W/\partial\theta^2 > 0$; if $\partial^2 W/\partial\theta^2 < 0$, the local crack development will be unstable [20]. The boundary between stability and instability is described by:

$$\partial^2 W/\partial\theta^2 = 0. \tag{10}$$

The extreme values can be readily determined from stability charts (the normalized crack-parallel stress α^* versus the angle θ_n) as shown in Figs.5-9. The evolution of the stability curves from the symmetric Mode-I case to the non-symmetric case of general mixed-mode is depicted in Fig.5 for a static crack under plane strain conditions with Poisson's ratio, $\nu = 0.25$. In the figure, thick (fine) lines correspond to stable (unstable) crack propagation, respectively. Notice that the Mode-II contribution to mixed-mode ($m = K_{II}/K_I$) is considered as a small disturbance to the Mode-I pattern, and that the resulting stability curves are similar to curves obtained in the analysis of imperfection sensitive elastic structures (see e.g. [19]). When $m = 0$ (Mode-I loading), only the section $\alpha^* \leq 1/6$ of the axis $\theta_n = 0°$ represents minima of the strain energy density which gives rise to directionally stable crack extension. However, when sufficiently large imperfect (shear mode-II) loading is added (e.g. $m = 0.25$), then the stability curves change its shape considerably [Fig.5(c)], indicating that under the action of sufficiently large imperfect loading, a crack can stably propagate regardless of the sign and magnitude of the uniform regular stress acting parallel to the crack line. In other words, adding mode-II loading will enhance the crack path stability.

The influence of the state of stress and varying Poisson's ratio onto the stability charts for a static Mode-I crack is shown in Fig.6. Figures 6(a)-(c) pertain to the plane strain conditions while the other figures (d)-(f) are related to the conditions of plane stress. The figures indicate that increasing Poisson's ratio will slightly enhance the directional stability of a crack and that plane strain conditions render more stable crack extension than plane stress conditions.

The perspective Lagrangian-type graphical representation, Fig.7, shows the effect of crack tip velocity and crack-parallel stress on mode-I crack path stability. In the figure, the coordinate axes denote the crack tip velocity normalized by the relevant shear wave speed, c/c_S,

the angle θ_n with respect to the crack line and the normalized crack-parallel stress α^*. In Fig.8, the projection of the curve of degenerate critical points on the α^*, c/c_S-plane is depicted for Mode-I stress loading. Figures 7, 8 and the dynamic stability diagrams for mode-I cracks, Figs.9(a)-(c), together with the catastrophe theory, indicate that:

- In general, also for a dynamically propagating crack, the positive (tensile) crack-parallel stress reduces the stability of crack path while negative (compressive) crack-parallel stress enhances the path directional stability;
- The stability curve changes its characteristic shape when the crack speed passes $c/c_S \approx 0.45$ ($c/c_R \approx 0.5$) and exceeds the limit to attain a stable bifurcation which allows for crack division; and
- The increase of crack tip propagation speed reduces the stabilizing effect of the crack-parallel stress: If a crack, for example, is under the slightly positive (tensile) crack-parallel stress such as indicated by the broken arrow in Fig.8, then this crack is stable in the range $c/c_S < 0.2$ ($c/c_R < 0.22$), becomes unstable with possible surface roughening between $0.2 < c/c_S < 0.45$ ($0.22 < c/c_R < 0.5$) and bifurcates when $c/c_S > 0.45$ ($c/c_R > 0.5$). If a crack is under the compressive crack-parallel stress marked by the solid arrow in Fig.8, the crack propagates stably in the range $c/c_S < 0.6$ ($c/c_R < 0.65$) and then stably bifurcates $c/c_S > 0.6$ ($c/c_R > 0.65$). In both cases, a crack cannot propagate without changing its surface configuration if the tip speed exceeds a certain limit. It should also be noted that slight change in the tensile crack-parallel stress will affect the crack surface roughening and/or branching velocity considerably.

The above results, in general, are in good agreement with the experimental as well as theoretical results summarized in the previous two chapters of this contribution.

The situation where a small directional imperfection ($m = K_{II}/K_I = 0.05$) is superimposed onto the running Mode-I crack is depicted in Figs.9(d)-(f). The stability curve for a medium crack tip velocity [Fig.9(e)] shows, like the static one (Fig.5), that under the action of imperfect loading, a crack can stably propagate regardless of the sign and magnitude of the crack-parallel stress. Comparison of Figs.9(b) and (e) suggests that the superimposition of mode-II loading will enhance the crack path stability also for dynamic cases. Again, this result is consistent with the experimentally observed phenomena (Figs.3 and 4). In the high-velocity range [Figs.9(c), (f)], the outside branches of the fork-type stability curve represent stable crack paths, which eventually may lead to (a)symmetric branching patterns. Again, the stability of a crack may be controlled by the sign and magnitude of the crack-parallel stress, or α- (α^*-) term.

Since different configurations of fracture test specimens are associated with differing α-(α^*-) values, crack path directional stability is essentially dependent on type and size of the cracked component. Practice shows that DCB-type components are most sensitive to imperfections and show extreme unstable dynamic fracture behavior like off-centerline deviation and subsequent tearing-off of one arm of the specimen [11]. Figure 8 shows that under the action of tensile crack-parallel stress, which is expected in DCB-type components, the regions of stable, unstable crack propagation and bifurcation are located very close to each other, suggesting that slight change of α (α^*) renders a totally different crack behavior. This is in good agreement with the practical observations described above.

4. Conclusions

Crack path directional stability has been considered based on the experimentally recorded photographs and the analytically obtained distributions of the maximum in-plane shear stress and the strain energy density in the vicinity of crack tips. The stability charts for Mode-I and mixed-

mode cracks, which have been analytically obtained by employing the strain energy density fracture criterion in connection with the catastrophe theory, have allowed for detailed discussion of the dynamic behavior of cracks: stable propagation; unstable, surface roughening propagation; and/or crack bifurcation. It has been shown that the crack-parallel stress considerably affects the directional stability of crack paths and its slight difference may be able to change the crack surface roughening and/or branching velocity, especially when the crack-parallel stress is tensile: the phenomena have been observed also practically in the DCB-type cracked components. It has also been pointed out that adding mode-II loading and/or decreasing crack tip propagation speed will enhance the dynamic crack path stability. Increasing Poisson's ratio will slightly enhance the directional stability of a crack, and conditions of plane strain will render more stable crack extension than plane stress conditions.

Acknowledgements

This work has been sponsored by the Austrian National Science Foundation under Project No. P10326-GEO.

References

[1] Broberg, K.B.: Cracks and Fracture, 752pp. San Diego: Academic Press 1999.

[2] Freund, L.B.: Dynamic Fracture Mechanics, 563pp. Cambridge: Cambridge University Press 1990.

[3] Ravi-Chandar, K., Knauss, W.G.: An experimental investigation into dynamic fracture. I. Crack initiation and crack arrest; II. Microstructural aspects; III. Steady state crack propagation and crack branching; IV. On the interaction of stress waves with propagating cracks. Int. J. Fracture **25**, 247 262; **26**, 65 80; **26**, 141 154; **26**, 189 200 (1984).

[4] Sharon, E., Gross, S.P., Fineberg, J.: Local crack branching as a mechanism for instability in dynamic fracture. Phys. Rev. Lett. **74**, 5096 5099 (1995).

[5] Sharon, E., Fineberg, J.: Microbranching instability and the dynamic fracture of brittle materials. Phys. Rev. B **54**, 7128 7139 (1996).

[6] Rice, J.R.: New perspectives on crack and fault dynamics. In: Mechanics for a New Millennium (Proceedings of the 20th International Congress on Theoretical and Applied Mechanics) (Aref, H., Phillips, J.W., eds.), pp.1-23, Dordrecht: Kluwer Academic Publishers, 2001.

[7] Yoffe, E.H.: The moving Griffith crack. Phil. Mag. **42**, 535 563 (1951).

[8] Freund, L.B.: Crack propagation in an elastic solid subject to general loading. I. Constant rate of extension; II. Non-uniform rate of extension. J. Mech. Phys. Solids **20**, 129 152 (1972).

[9] Rossmanith, H.P., Irwin, G.R.: Analysis of Dynamic Isochromatic Crack-Tip Stress Patterns, University of Maryland Report 1979.

[10] Rossmanith, H.P.: Analysis of mixed-mode isochromatic crack-tip fringe patterns. Acta Mech. **34**, 1 38 (1979).

[11] Rossmanith, H.P.: Crack propagation and branching. In: Proceedings of an International Symposium on Absorbed Specific Energy and/or Strain Energy Density Criterion (Sih, G.C., Czoboly, E., Gillemot, F., eds.), pp.283 294, Budapest: Akadémiai Kiadó, 1981.

[12] Uenishi, K., Rossmanith, H.P.: The effect of crack-parallel stress and mixed-mode loading on dynamic crack path instability. Eos Trans. AGU **81(48)**, F1238 F1239 (2000).

[13] Melin, S.: Why do cracks avoid each other? Int. J. Fracture **23**, 37 45 (1983).

[14] Melin, S.: Directional stability of an originally straight crack. Int. J. Fracture **53**, 121 128 (1992).

[15] Cotterell, B., Rice, J.R.: Slightly curved or kinked cracks. Int. J. Fracture **16**, 155 169 (1980).

[16] Erdogan, F., Sih, G.C.: On the crack extension in plates under plane loading and transverse shear. J. Basic Engng **85**, 519 523 (1963)

[17] Freund, L.B., Clifton, R.J.: On the uniqueness of plane elastodynamic solutions for running cracks. J. Elasticity **4**, 293 299 (1974).

[18] Liu, C., Rosakis, A.J.: On the higher order asymptotic analysis of a non-uniformly propagating dynamic crack along an arbitrary path. J. Elasticity **35**, 27 60 (1994).

[19] Poston, T., Stewart, I.: Catastrophe Theory and Its Applications, 491pp. London: Pitman 1978.

[20] Cherepanov, G.P., Germanovich, L.N.: An employment of the catastrophe theory in fracture mechanics as applied to brittle strength criteria. J. Mech. Phys. Solids **41**, 1637 1649 (1993).

Figure Legends

Figure 1. Geometrical configuration of a mixed-mode crack propagating dynamically.

Figure 2. Schematic view of (a) Double-Cantilever-Beam (DCB) specimen; and (b) Single-Edge-Notched (SEN) specimen. DCB gives positive (tensile) crack-parallel stress while SEN renders negative (compressive) normal stress acting parallel to the crack surface.

Figure 3. Experimentally recorded and analytically generated dynamic isochromatic fringe patterns (contours of in-plane maximum shear stress) and strain energy density distributions around a moving crack tip (c/c_S = 0.2) subjected to Mode-I ($m = K_{II}/K_I$ = 0; left column) and mixed-mode (m = 0.1; right column) stress loading in a Double-Cantilever-Beam specimen (α = 1.0, ν = 0.25).

Figure 4. Isochromatic fringe patterns and strain energy density distributions around a dynamically propagating crack tip (c/c_S = 0.2) under Mode-I ($m = K_{II}/K_I$ = 0; left column) and mixed-mode (m = 0.1; right column) stress loading in a Single-Edge-Notched specimen (α = –1.0, ν = 0.25), obtained experimentally as well as analytically.

Figure 5. Stability chart (α^* [$= \sigma_x^\infty \sqrt{2\pi r_n} \big/ K_I$] versus θ_n) associated with the equi-strain-energy-density line patterns for a *static* crack subjected to various combined mode stress conditions [ν = 0.25; plane strain; $m = K_{II}/K_I$ = (a) 0, (b) 0.05, (c) 0.25; **thick lines**: stable, fine lines: unstable].

Figure 6. Influence of the state of stress and varying Poisson's ratio [ν = (a, d) 0, (b, e) 0.25, (c, f) 0.5] onto the stability chart (α^* versus θ_n) associated with equi-strain-energy-density line patterns for a *static* crack subjected to Mode-I conditions of (a, b, c) plane strain and (d, e, f) plane stress; **thick lines**: stable, fine lines: unstable.

Figure 7. Perspective representation of α^*–c/c_S–θ_n relationship. (Mode-I propagating crack; ν = 0.25; plane strain). The increase of crack tip propagation speed reduces the stabilizing effect of the crack-parallel stress.

Figure 8. The projection of the curve of degenerate critical points on the α^*, c/c_S-plane (Mode-I stress loading; ν = 0.25; plane strain).

Figure 9. *Dynamic* stability chart (α^* versus θ_n) associated with equi-strain-energy-density line patterns for a combined mode crack [$m = K_{II}/K_I$ = (a, b, c) 0, (d, e, f) 0.05; ν = 0.25; plane strain; c/c_S = (a, d) 0, (b, e) 0.4, (c, f) 0.6; **thick lines**: stable, fine lines: unstable].

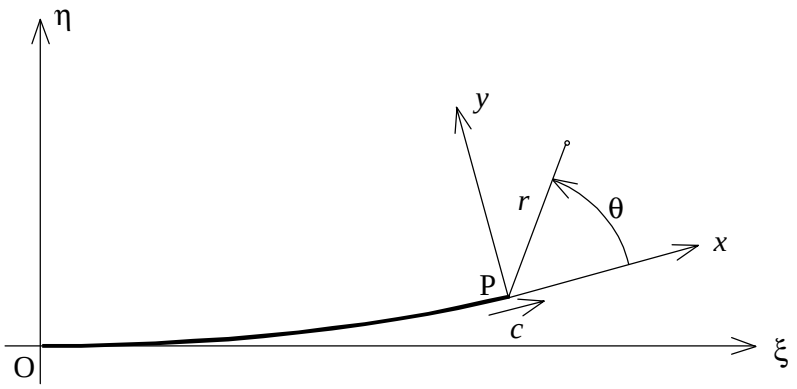

Figure 1. Geometrical configuration of a mixed-mode crack propagating dynamically.

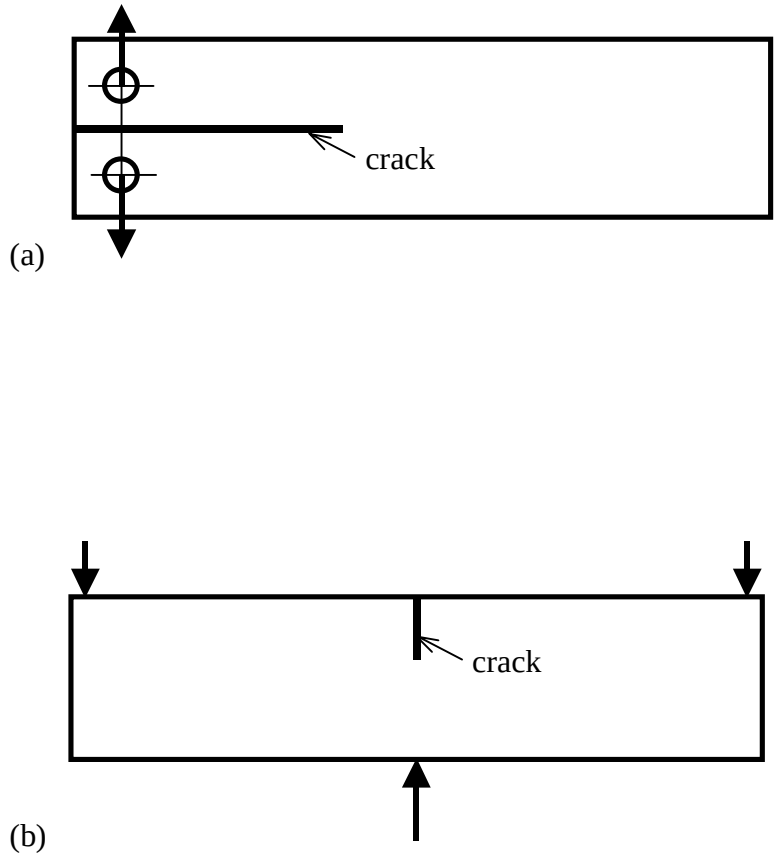

Figure 2. Schematic view of (a) Double-Cantilever-Beam (DCB) specimen; and (b) Single-Edge-Notched (SEN) specimen. A DCB specimen gives positive (tensile) crack-parallel stress while an SEN specimen renders negative (compressive) normal stress acting parallel to the crack surface.

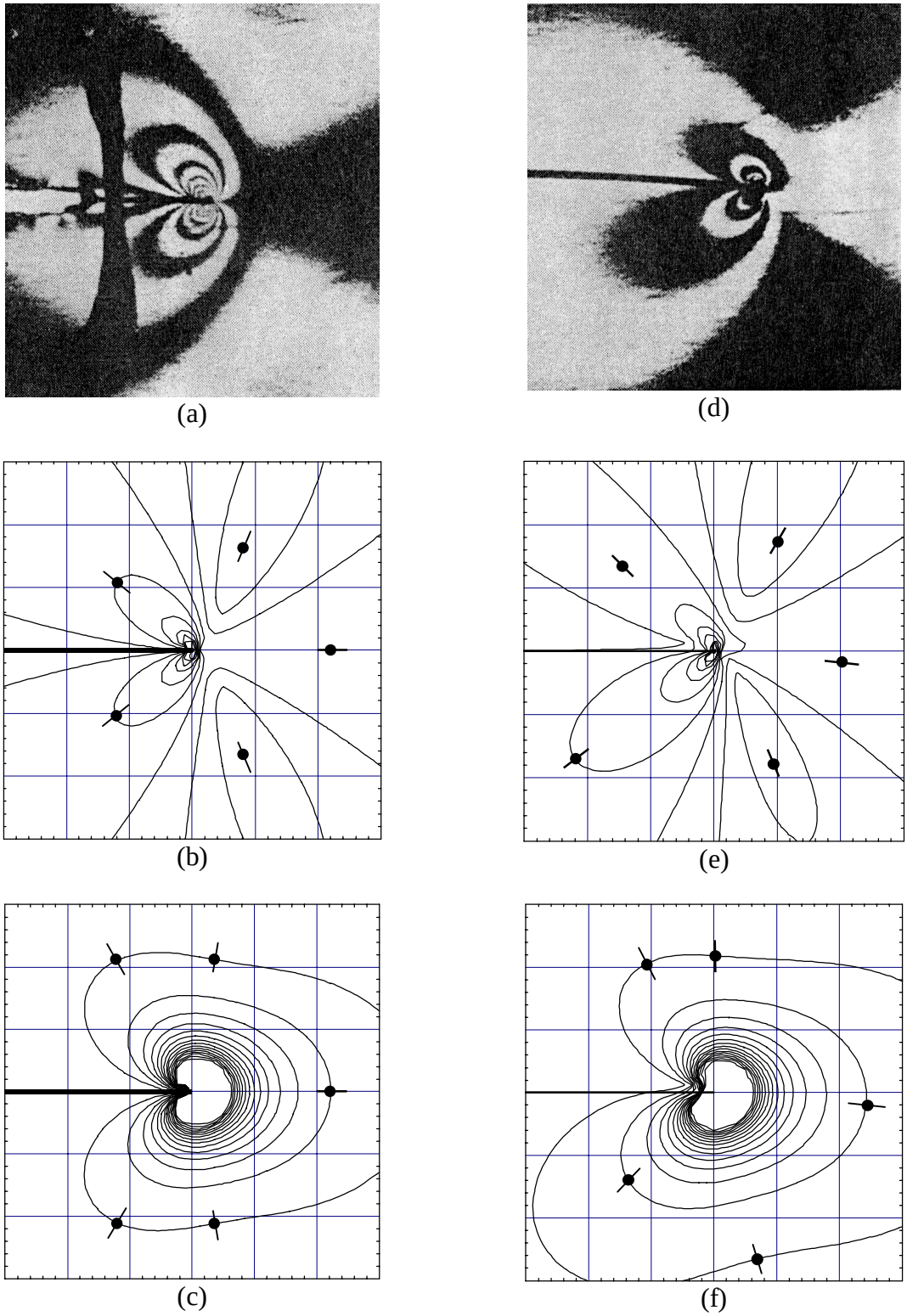

Figure 3. Experimentally recorded and analytically generated dynamic isochromatic fringe patterns (contours of in-plane maximum shear stress) and strain energy density distributions around a moving crack tip (c/c_S = 0.2) subjected to Mode-I ($m = K_{II}/K_I$ = 0; left column) and mixed-mode (m = 0.1; right column) stress loading in a Double-Cantilever-Beam specimen (α = 1.0, ν = 0.25).

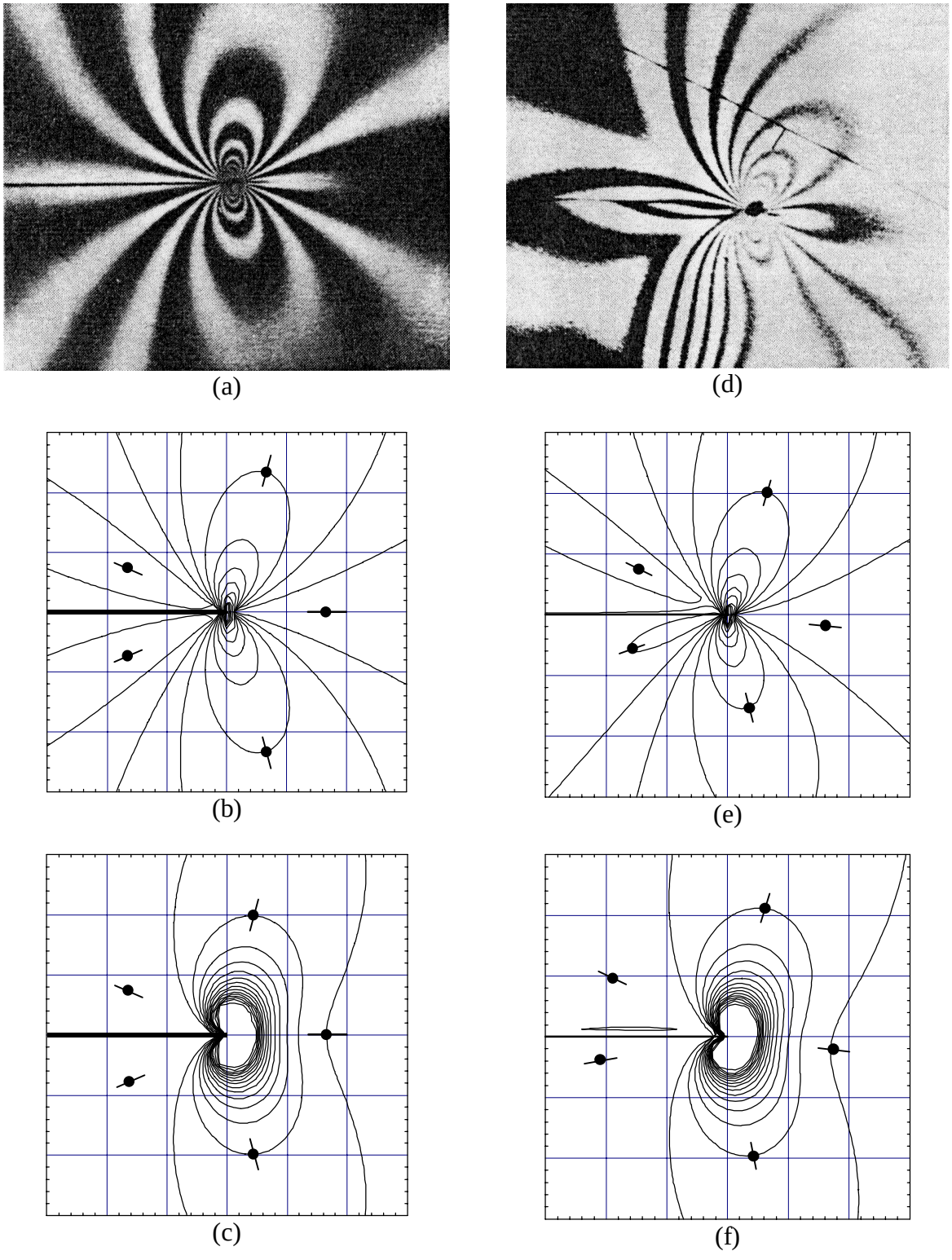

Figure 4. Isochromatic fringe patterns and strain energy density distributions around a dynamically propagating crack tip (c/c_S = 0.2) under Mode-I ($m = K_{II}/K_I = 0$; left column) and mixed-mode (m = 0.1; right column) stress loading in a Single-Edge-Notched specimen ($\alpha = -1.0$, $\nu = 0.25$), obtained experimentally as well as analytically.

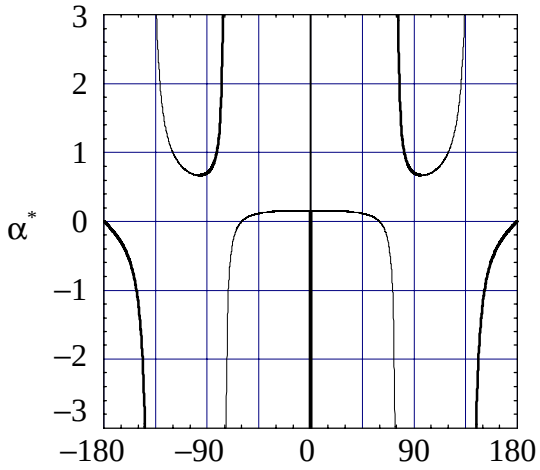

(a) m = 0

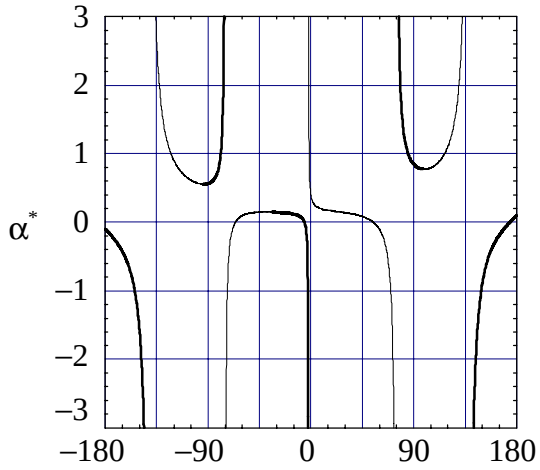

(b) m = 0.05

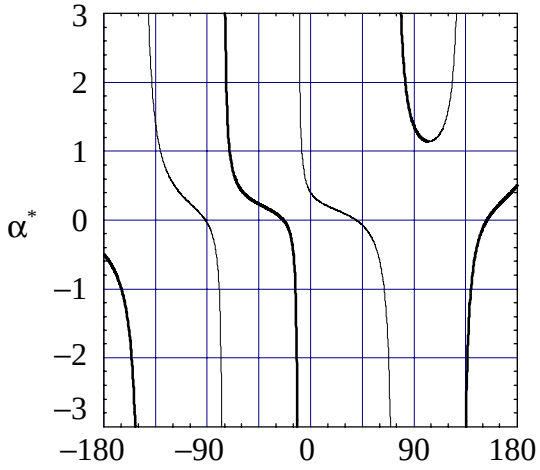

(c) m = 0.25

Figure 5. Stability chart (α^* [$= \sigma_x^\infty \sqrt{2\pi r_n} \big/ K_I$] versus θ_n) associated with the equi-strain-energy-density line patterns for a *static* crack subjected to various combined mode stress conditions [ν = 0.25; plane strain; $m = K_{II}/K_I$ = (a) 0, (b) 0.05, (c) 0.25; **thick lines**: stable, fine lines: unstable].

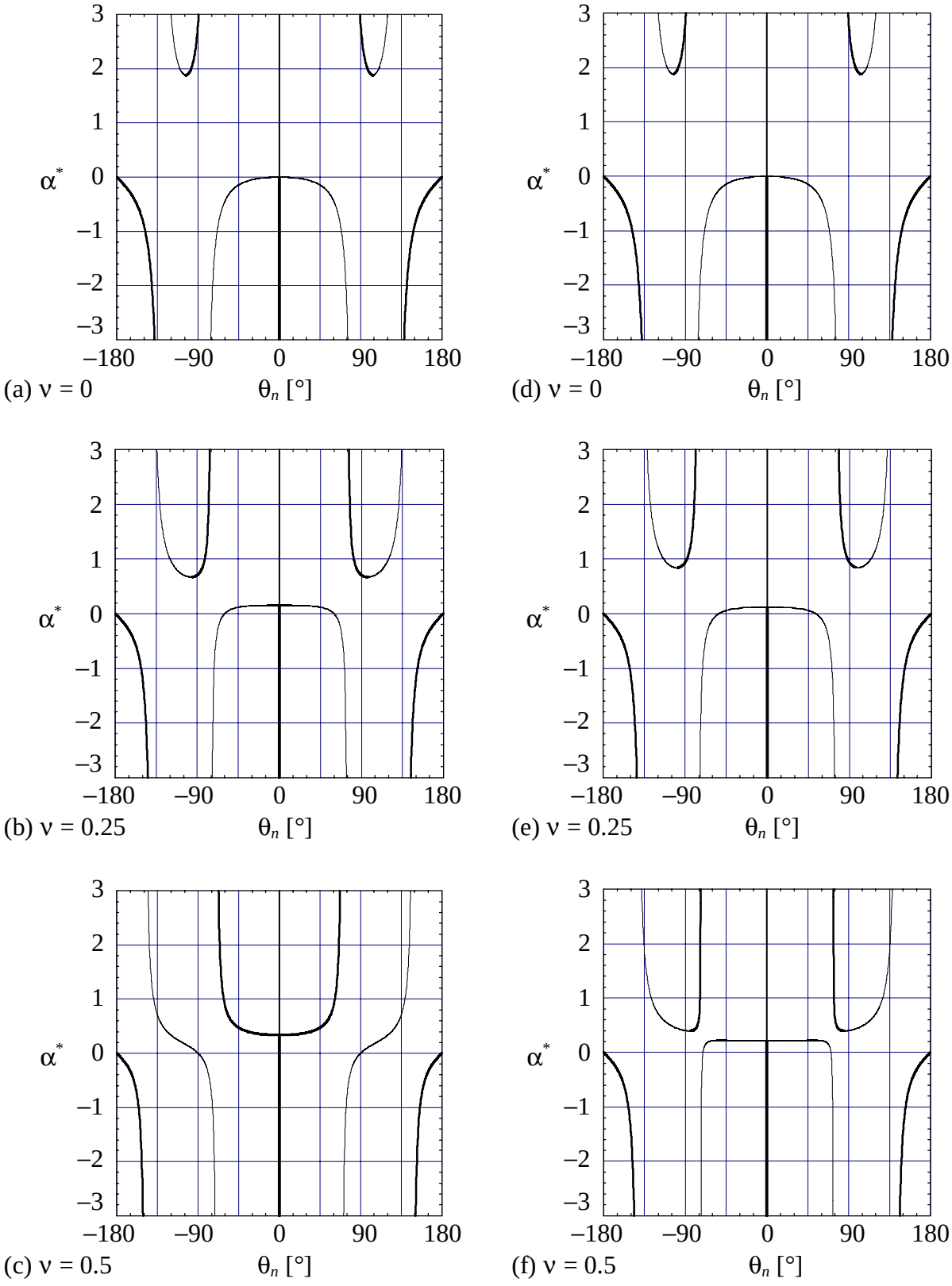

Figure 6. Influence of the state of stress and varying Poisson's ratio [ν = (a, d) 0, (b, e) 0.25, (c, f) 0.5] onto the stability chart (α^* versus θ_n) associated with equi-strain-energy-density line patterns for a *static* crack subjected to Mode-I conditions of (a, b, c) plane strain and (d, e, f) plane stress; **thick lines**: stable, fine lines: unstable.

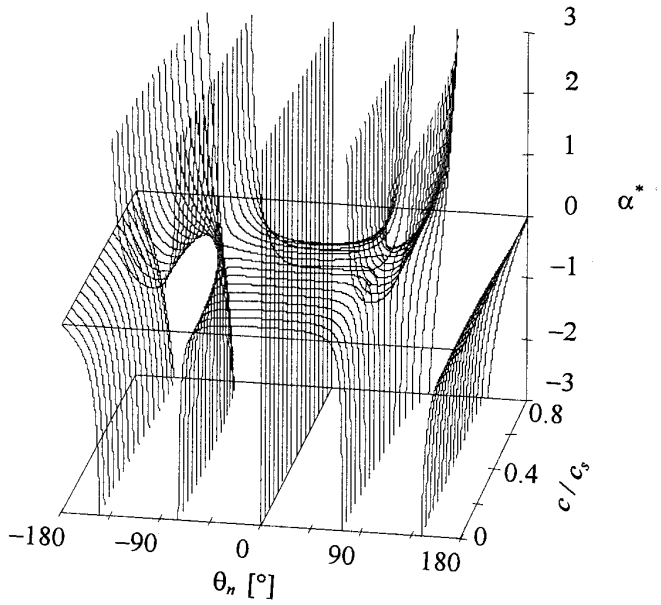

Figure 7. Perspective representation of α^{*}–c/c_S–θ_n relationship. (Mode-I propagating crack; $\nu = 0.25$; plane strain).

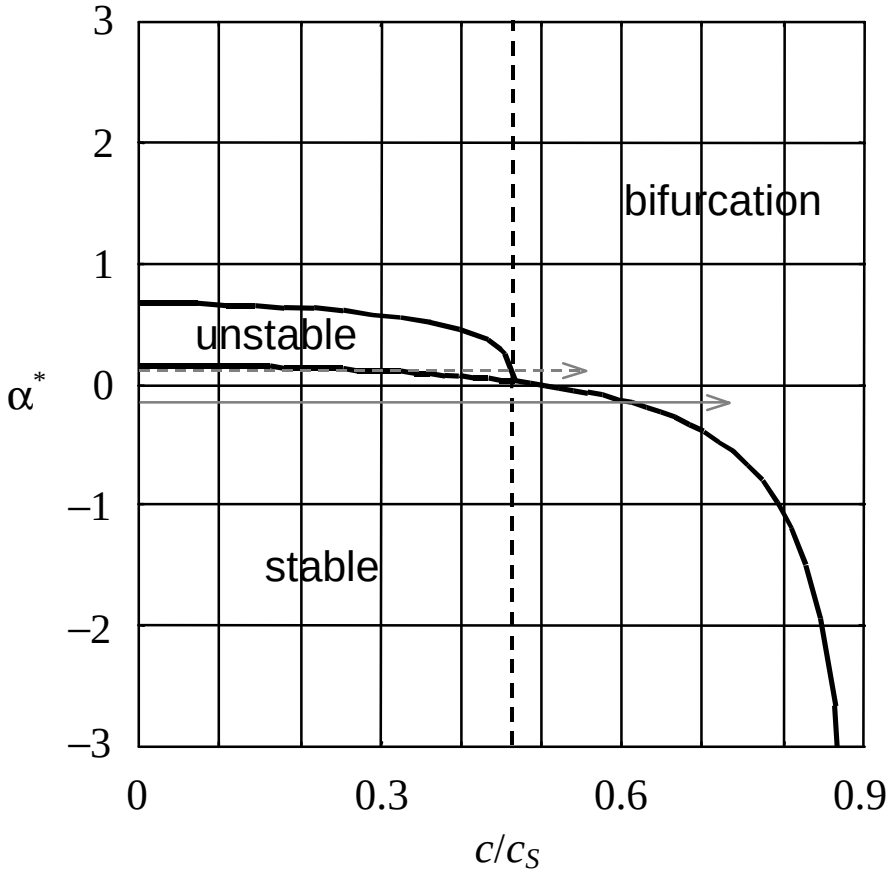

Figure 8. The projection of the curve of degenerate critical points on the α^*, c/c_S-plane (Mode-I stress loading; $\nu = 0.25$; plane strain). The increase of crack tip propagation speed reduces the stabilizing effect of the crack-parallel stress.

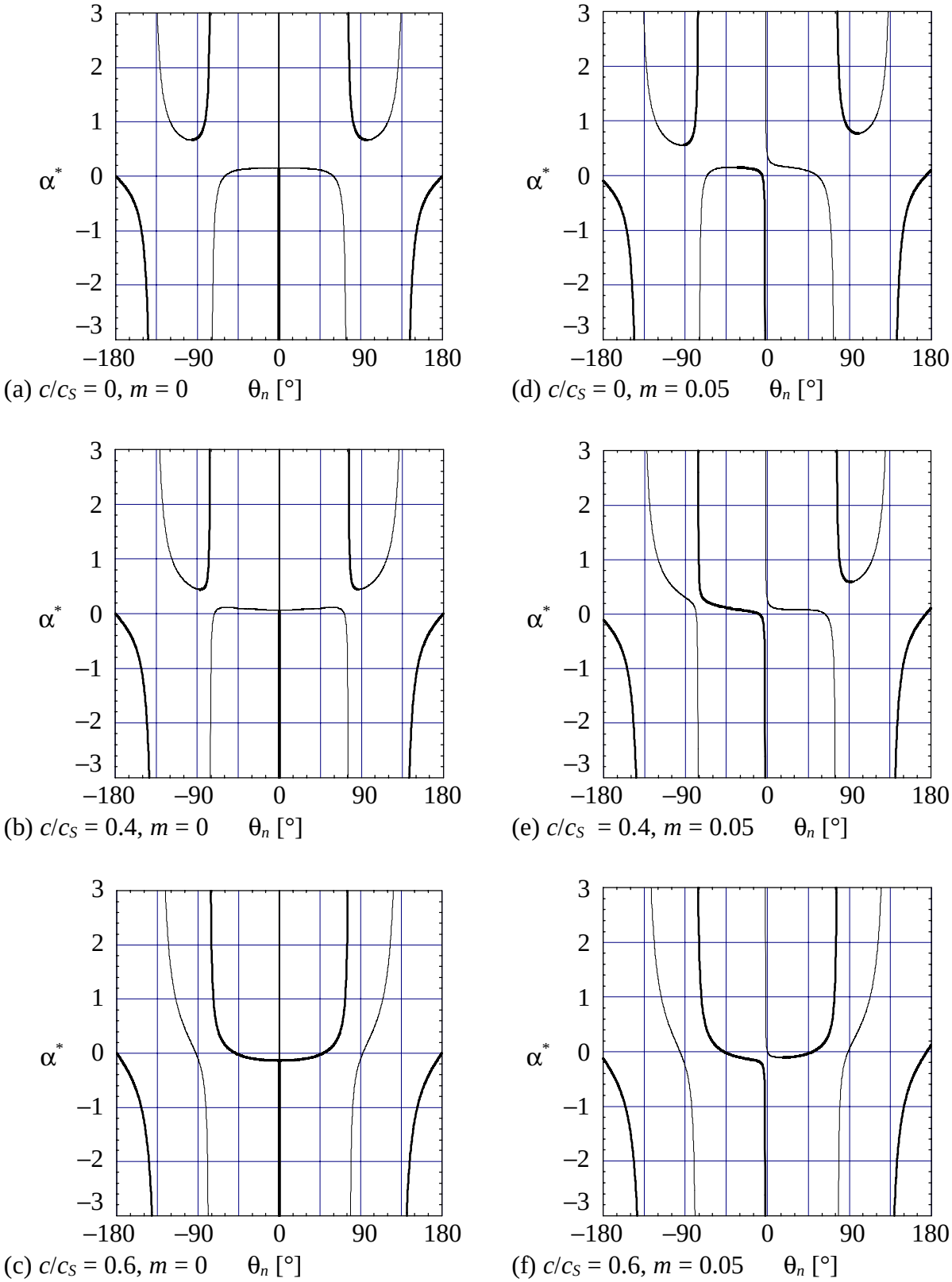

(a) $c/c_S = 0$, $m = 0$ (d) $c/c_S = 0$, $m = 0.05$

(b) $c/c_S = 0.4$, $m = 0$ (e) $c/c_S = 0.4$, $m = 0.05$

(c) $c/c_S = 0.6$, $m = 0$ (f) $c/c_S = 0.6$, $m = 0.05$

Figure 9. *Dynamic* stability chart (α^* versus θ_n) associated with equi-strain-energy-density line patterns for a combined mode crack [$m = K_{II}/K_I$ = (a, b, c) 0, (d, e, f) 0.05; $\nu = 0.25$; plane strain; c/c_S = (a, d) 0, (b, e) 0.4, (c, f) 0.6; **thick lines**: stable, fine lines: unstable].